Supporting Information

Ma et al. 10.1073/pnas.1201724109

Materials and Methods

Cell Culture and Transport Conditions. A HeLa cell line stably expressing the GFP-conjugate of POM121 was used, and freshly split cells were grown overnight on coverslips in DMEM supplemented with 10% FBS. For microscopy, flow chambers were constructed with a top cover-slip and two lines of silicone grease as spacers. Cells were washed with transport buffer (20 mM HEPES, 110 mM KOAc, 5 mM NaOAc, 2 mM MgOAc, 1 mM EGTA, pH 7.3), permeabilized for two minutes with 40 μg/mL digitonin in transport buffer, and washed again with transport buffer supplemented with 1.5% polyvinylpyrrolidone (PVP; 360 kDa). PVP was included in all transport buffer solutions after digitonin treatment to prevent osmotic swelling of the nuclei. For single-molecule measurements of transport receptors and passive diffusion of various molecules, 1 nM intrinsic fluorescent or dye-labeled substrates were used. For the efficient nuclear import of 1 nM labeled NLS-2xGFP at 0.5 μM, 3 μM and 15 μM Imp β1, the buffer contained the import cofactors 1 mM GTP, 2 μM Ran, 1 μM NTF2 and 0.5 μM, 3 μM or 15 μM Imp β1 and Imp α, respectively. More details can be found in previously published methods (1–5).

Dyes, Dextran, Proteins, and Labeling. Fluorescein, Alex Fluor 647 and dye-labeled dextrans were purchased from Invitrogen. Insulin and α-lactalbumin were bought from Sigma-Aldrich. N-terminal His-tagged GFP, NTF2, Imp β1 and transportin proteins were expressed in *Escherichia coli* and purified by Ni-NTA Superflow (Qiagen), MonoQ and Superdex 200 (Amersham) chromatography. The model substrate of NLS-2xGFP and the other transport cofactors were purified as described in previous reports (1–5), unless specified in *Materials and Methods*. The solvent-accessible cysteines on the proteins were labeled with 20-fold molar excess Alexa Fluor 647 maleimide dye (Invitrogen) for 2 h at room temperature in 50 mM sodium phosphate, 150 mM NaCl, pH 7.5. Reactions were quenched with β-mercaptoethanol, and the products were dialyzed to remove the free dyes. The labeling ratio is 1 dye per protein molecule for GFP, NTF2, insulin and α-lactalbumin, 2 dyes per transportin molecule, and 4 dyes per protein molecule for Imp β1 and NLS-2xGFP.

Dye Effect on the Function of Imp β1 and the Import Cargo Complex. The effect of dyes on the interactions between the labeled import cargo complex and the NPC have been previously investigated using transport rate measurements and shown to be negligible (1–4). By the same method, import rates of NLS-2xGFP in the presence of unlabeled or labeled-Imp β1 molecules were measured, and the same transport rates were obtained in both cases. Therefore, the labeled dyes on Imp β1 or NLS-2xGFP are unlikely to affect the functions of the substrates through interactions with the FG repeats along the NPC.

Single-GFP-POM121 Cell Line. By conjugating GFPs with POM121, the middle plane of the nuclear envelope can be determined (1, 2). However, multiple-GFPs-conjugate-POM121 NPCs have enhanced transport time and efficiency compared to that of wild-type (WT) NPCs (4). Following the same experimental procedure, the transport time and efficiency for single-GFP-POM121 NPCs was measured, and it was found that nuclear transport was not enhanced by a single GFP-conjugate. Therefore, experiments were conducted with a single-GFP-POM121 cell line, and GFP fluorescence was utilized to localize the centroid of individual NPC.

Orientation of a Single NPC. The position of the nuclear envelope (NE) was localized by fitting GFP fluorescence of POM121 as follows: The pixel intensities within a row or a column approximately perpendicular to the NE were fit to a Gaussian. The peak position of the Gaussian for a particular set of pixel intensities was considered the NE position for that row and column. The peak positions of a series of such Gaussians were then fit with a second-degree polynomial, yielding the path of the NE within the entire image (1).

Two rules were then used to select a single NPC oriented perpendicularly to the NE on the equator of the nucleus and to the y direction of the Cartesian coordinates (x, y) in the CCD camera: (*i*) Choose a fluorescent NPC on the equator of the nucleus such that the tangent of the NE at the location of this NPC should be parallel to the y direction of the Cartesian coordinates (x, y) in the CCD camera; and (*ii*) examine the ratio of Gaussian widths in the long and short axes of the chosen GFP-NPC fluorescence spot. The ratio needs to fall between 1.74 and 1.82. Within this range, an illuminated NPC only has a free angle of 1.4° to the perpendicular direction to the NE (1).

Instrumentation. The SPEED microscope includes an Olympus IX81 equipped with a 1.4 NA 100× oil-immersion apochromatic objective (UPLSAPO 100X, Olympus), a 35 mW 633 nm He-Ne laser (Melles Griot), a 120 mW ArKr tunable ion laser (Melles Griot), an on-chip multiplication gain charge-coupled device camera (Cascade 128+, Roper Scientific) and the Slidebook software package (Intelligent Imaging Innovations) for data acquisition and processing. An optical chopper (Newport) was used to generate an on-off mode of laser excitation. Fluorescein, GFP, Alexa Fluor 488 and Alexa Fluor 647 fluorescence were excited by 488 nm and 633 nm lasers, respectively. The two lasers were combined by an optical filter (FFF555/646 Di01, Semrock), collimated and focused into an overlapped illumination volume in the focal plane. The green and red fluorescence emissions were collected by the same objective, filtered by a dichroic filter (Di01-R405/488/561/635-25x36, Semrock) and an emission filter (NF01-405/488/561/635-25X5.0, Semrock) and imaged by an identical CCD camera. The system error of alignment between red and green fluorescence channels is 3.0 ± 0.1 nm, determined by measuring 230 immobile Alexa Fluor 647-labeled GFP fluorescent molecules on the surface of a cover-slip.

Localization Precisions of Isolated Fluorescent Spots. The localization precision for fluorescent NPCs, immobile fluorescence molecules and moving fluorescence molecules was defined as how precisely the central point of each detected fluorescent diffraction-limited spot was determined. For immobile molecules or fluorescent NPCs, the fluorescent spot was fitted to a 2D symmetrical or an elliptical Gaussian function, respectively, and the localization precision was determined by the standard deviation of multiple measurements of the central point. However, for moving molecules, the fluorescent spot was fitted to 2D elliptical Gaussian functions, but the localization precision (σ) was determined by an algorithm of $\sigma = \sqrt{\frac{s^2}{N} + \frac{a^2}{12N} + \frac{8\pi s^4 b^2}{a^2 N^2}}$, where N is the number of collected photons, a is the effective pixel size of the detector, b is the standard deviation of the background in photons per pixel, and s is the standard deviation of the point spread function (6).

To justify the precision obtained by the standard deviation of multiple measurements and the algorithm, both methods were used to determine the localizations of immobile fluorescent

molecules (Alexa Fluor 647-labeled-Imp β1 absorbed on the surface of a cover-slip) and fluorescent NPCs. A total of 155 immobile labeled-Imp β1 molecules were measured, and the two methods yielded a difference of 0.4 ± 0.1 nm. Based on 24 NPCs, the two methods generated a difference of 0.3 ± 0.1 nm. As shown in Table S1, the localization precision is approximately 9–12 nm for the immobile molecules and 10–13 nm for the moving molecules when around 1,100 photons were collected from the targeted molecule.

Determination of Molecular Diameter. Permeation probes used as in this paper meet a number of criteria: (*i*) For proteins, a compactly folded domain with nearly spherical shape and no interactions with NPC are needed. (*ii*) For dyes or dextran molecules, they have been used to test the NPC permeability before. (*iii*) Their molecular diameters have been measured experimentally by gel filtration or size exclusion column. (*iv*) Contribution of labeled dyes on the substrate for the final size of substrate was determined by the relationship between diameter (d) and molecular weight (MW) with (w) or without (o) labeled dyes as $\frac{d_w}{d_o} = (\frac{MW_w}{MW_0})^{-3}$.

Gaussian Fittings in the Determination of Dimensions for Transport Routes in the NPC. The obtained spatial probability density distribution of transiting molecules in the NPC were fitted by one or multiple Gaussian functions. From the Gaussian fittings, the spatial dimension of transport route was determined. For example, as shown in Fig. 3, the length and diameter of the central passive diffusion channel in the NPC were determined by Gaussian fitting. However, the obtained Gaussian width cannot be directly used to characterize the dimension of transport passageway, and the effects of single-molecule localization precision and the molecular size should be included in the final determination of dimensions of transport pathways. Thus, in detail, the e^{-1}, full width at half maximum (FWHM) or e^{-2} width (W_o) of a Gaussian function was corrected by including the localization precision of single molecules (σ_s) and the molecular diameter (d_s) as follows: $W_c = \sqrt{W_O^2 - \sigma_S^2} + d_s$, where W_c is the corrected width. For passive diffusion of small molecules, W_c represented the diameter or the length of the central channel. However, the diameters of the tubes rarely occupied by Imp β1 and the import cargo complexes were further determined by W_c and the peak position (P) of Gaussian fitting of probability density distribution of interactions sites in the NPC. Finally, the diameter of unoccupied tube was obtained as $2P - W_c$.

As indicated by Gaussian fittings in both axial and radial directions for passive diffusion routes in Fig. 3 *A*–*C* (the detected transiting molecules were included in the e^{-1}, FWHM, and e^{-2} widths of Gaussian fitting with approximately 68%, 76%, and 95% probability, respectively), the determined diameter and length of the central channel strongly depended on the molecular size and the dependency relationships were subsequently fitted by exponential functions (Fig. 3*D*). For example, those larger molecules (approximately 3–7 nm in diameter) passively diffused through the NPC via a central channel with approximately 17–19 nm in diameter at the narrowest point (11–12 nm and 12–13 nm at the e^{-1} and FWHM widths, respectively) and about 140–179 nm in length based on the e^{-2} width of Gaussian fit (70–89 nm and 83–106 nm at the e^{-1} and FWHM widths, respectively) (Fig. 3*D* and Table S2). The above determined dimensions of the central channel agree with previous results obtained from EM measurements or bulk nucleocytoplasmic transport rates (8–11). However, smaller molecules ($< \sim 3$ nm in diameter) further diffused beyond such a spatial definition and could partition into more or even entire space of the peripheral FG-Nups-transport receptor interacting regions in either the axial or the radial direction inside the NPC (Fig. 3*D*). Additionally, the farther diffusion of smaller molecules may suggest that the central channel unlikely has an "impermeable solid wall" but rather a "permeable selective wall."

Determination of the Effective Viscosity of Medium in the Central Passive Diffusion Channel. Comparisons between the measured nucleocytoplasmic transport time (τ) and the calculated time (t) of various small molecules showed that the effective viscosity ($\eta_{\text{pore}} = \frac{\tau}{t} * \eta_{\text{aqueous}}$) of the medium in the central passive diffusion channel ranged from 1.6–3.4 cp, which is much larger than the viscosity of our import buffer ($\eta_{\text{aqueous}} = 1$ cp) in an aqueous open channel (Fig. 3 *E* and *F*). In detail, the diffusion time (τ) of small molecules through the NPC was measured by counting the dwell time in the NPC based on their single-molecule tracking trajectories (as τ in Fig. 1*G*). The calculated time (t) was determined from the mean squared displacements as $t = \frac{\langle \delta_{\text{axis}}^2(t) \rangle}{2A_c D_{\text{axis}}}$, where δ_{axis} is a instantaneous moving distance projected along the axis of NPC, $\langle \delta_{\text{axis}}^2(t) \rangle$ is the measured length of central channel, A_c is the spatial confinement effect of the nuclear pore on inserted molecules (7), and $D_{\text{axis}}\left(\propto \frac{1}{\eta_{\text{aqueous}}}\right)$, is the projected diffusion coefficient of transiting substrates through an aqueous channel along the NPC axis. Obviously, 3D dimension of the central passive diffusion tube varied for different-sized passively transiting molecules. Based on the ratio of measured and calculated transport times, we further found that the viscosity of the medium in the central passive diffusion tube for smaller molecules (approximately 1–3 nm in diameter) (η_{pore}) increased approximately two times than that for larger molecules (approximately 3–7 nm in diameter) (Fig. 3*F* and Table S2).

Intervenes Between Passive and Facilitated Transport. Intervenes between passive and facilitated transport in the NPC were observed in some studies but not in others (12–14). The obtained data in this paper can provide the following insight into this dispute: (*i*) Though passive diffusion and facilitated translocation possess mainly separate pathways in the NPC, these two transport zones are not completely forbidden areas to each other. The overlapped space between them depends on the size of transiting molecules. For example, the routes between larger facilitated translocation cargo complex and smaller passively diffusion molecules would have more overlaps; thus, they could affect each other more significantly under the circumstance. (*ii*) Concentrations of transport receptors (i.e., Imp β1) and RanGTP presented in the transport system can greatly affect the dimensions of passageways and the transport rates for both passive and facilitated transport. Thus, different concentrations of transport receptors adopted in the previous experiments could make completely different conclusions, although the same type of transport receptors were used in those experiments.

Deconvolution and Image Processing. The detailed deconvolution process used to obtain the 3D spatial distribution of transiting molecules in the NPC was described in our previous publication (1). The three-dimensional, surface-rendered visualizations in Figs. 2–4, Figs. S3–S6, and Movies S6–S10 were treated with Amira 5.2 (Visage Imaging).

Standard Error. Experimental measurements are reported as means ± standard errors of the mean unless otherwise noted.

1. Ma J, Yang W (2010) Three-dimensional distribution of transient interactions in the nuclear pore complex obtained from single-molecule snapshots. *Proc Natl Acad Sci USA* 107:7305–7310.

2. Yang W, Gelles J, Musser SM (2004) Imaging of single-molecule translocation through nuclear pore complexes. *Proc Natl Acad Sci USA* 101:12887–12892.

3. Yang W, Musser SM (2006) Visualizing single molecules interacting with nuclear pore complexes by narrow-field epifluorescence microscopy. *Methods* 39:316–328.
4. Yang W, Musser SM (2006) Nuclear import time and transport efficiency depend on importin beta concentration. *J Cell Biol* 174:951–961.
5. Sun C, Yang W, Tu LQ, Musser SM (2008) Single-molecule measurements of importin alpha/cargo complex dissociation at the nuclear pore. *Proc Natl Acad Sci USA* 105:8613–8618.
6. Thompson RE, Larson DR, Webb WW (2002) Precise nanometer localization analysis for individual fluorescent probes. *Biophys J* 82:2775–2783.
7. Cui ST (2005) Molecular self-diffusion in nanoscale cylindrical pores and classical Fick's law predictions. *J Chem Phys* 123:054706 1–4.
8. Rout MP, et al. (2000) The yeast nuclear pore complex: Composition, architecture, and transport mechanism. *J Cell Biol* 148:635–651.
9. Fahrenkrog B, Aebi U (2003) The nuclear pore complex: Nucleocytoplasmic transport and beyond. *Nat Rev Mol Cell Biol* 4:757–766.
10. Macara I G (2001) Transport into and out of the nucleus. *Microbiol Mol Biol Rev* 65:570–594.
11. Peters R (2005) Translocation through the nuclear pore complex: selectivity and speed by reduction-of-dimensionality. *Traffic* 6:421–427.
12. Hinshaw J E, Carragher B O, Milligan R A (1992) Architecture and design of the nuclear pore complex. *Cell* 69:1133–1141.
13. Fiserova J, Richards SA, Wente SR, Goldberg MW (2010) Facilitated transport and diffusion take distinct spatial routes through the nuclear pore complex. *J Cell Sci* 123:2773–2780.
14. Mohr D, Frey S, Fischer T, Guttler T, Gorlich D (2009) Characterization of the passive permeability barrier of nuclear pore complexes. *EMBO J* 28:2541–2553.

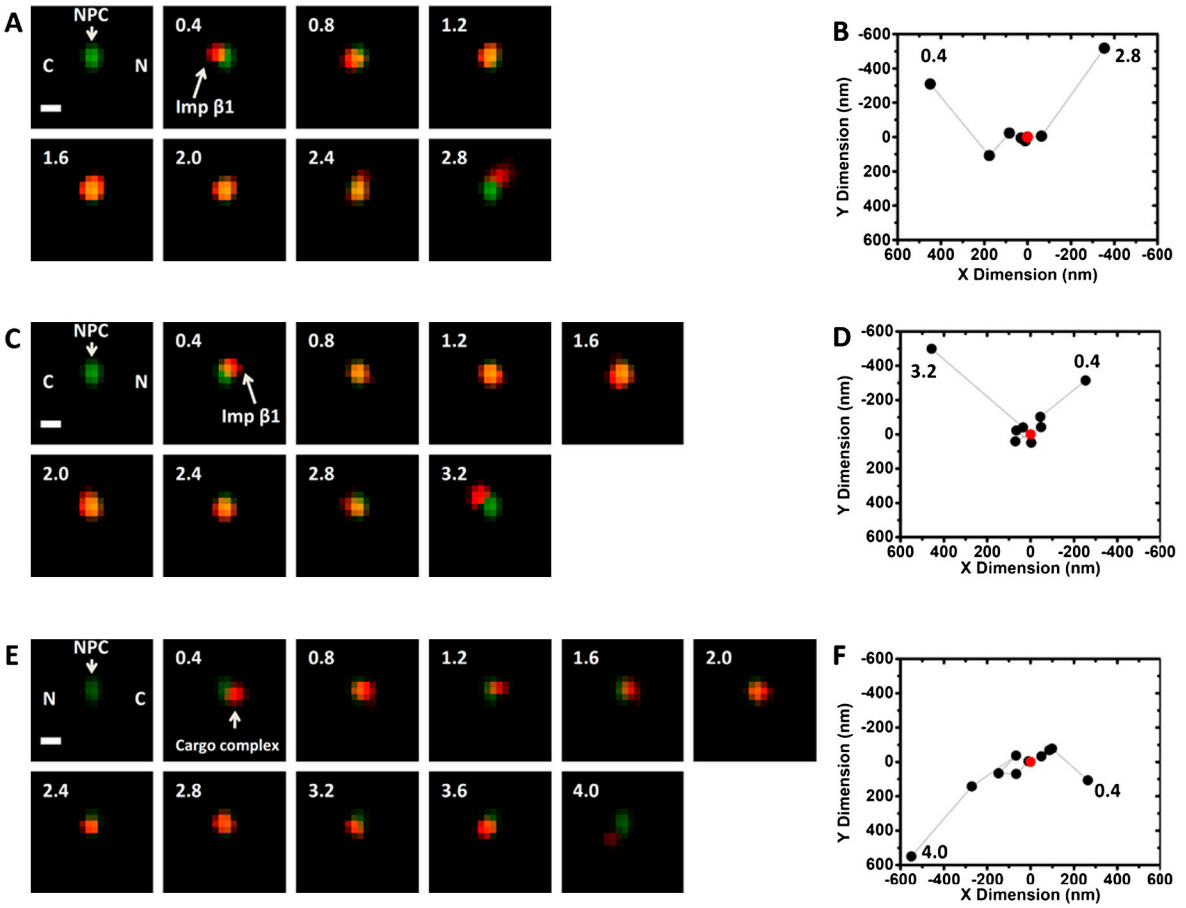

Fig. S1. Single-molecule trajectories of typical nucleocytoplasmic transport events of Imp β1 and import cargo complex Imp α/Imp β1/NLS-2xGFP obtained by SPEED microscopy. (*A*) A typical nuclear import event of Imp β1 molecules from the cytoplasm to the nucleus. First, a single GFP-NPC (green spot) was visualized in the illumination volume. Then, a single fluorescent Imp β1 molecule (red spot) entered the illumination volume, started in the cytoplasm (C), interacted with the NPC and entered the nucleus (N). Numbers denote time in millisecond. Scale bar: 1 μm. (*B*) Single-molecule trajectories of the import event in *A*. Based on the centroid (red dot) and the dimensions of the NPC, the spatial locations of Imp β1 molecule from 1.2 ms to 2.4 ms was within the NPC. (*C* and *D*) Individual video frames and the corresponding single-molecule trajectories of a typical export event for Imp β1. (*E* and *F*) Individual video frames and the corresponding single-molecule trajectories of a typical import event for the import cargo complex.

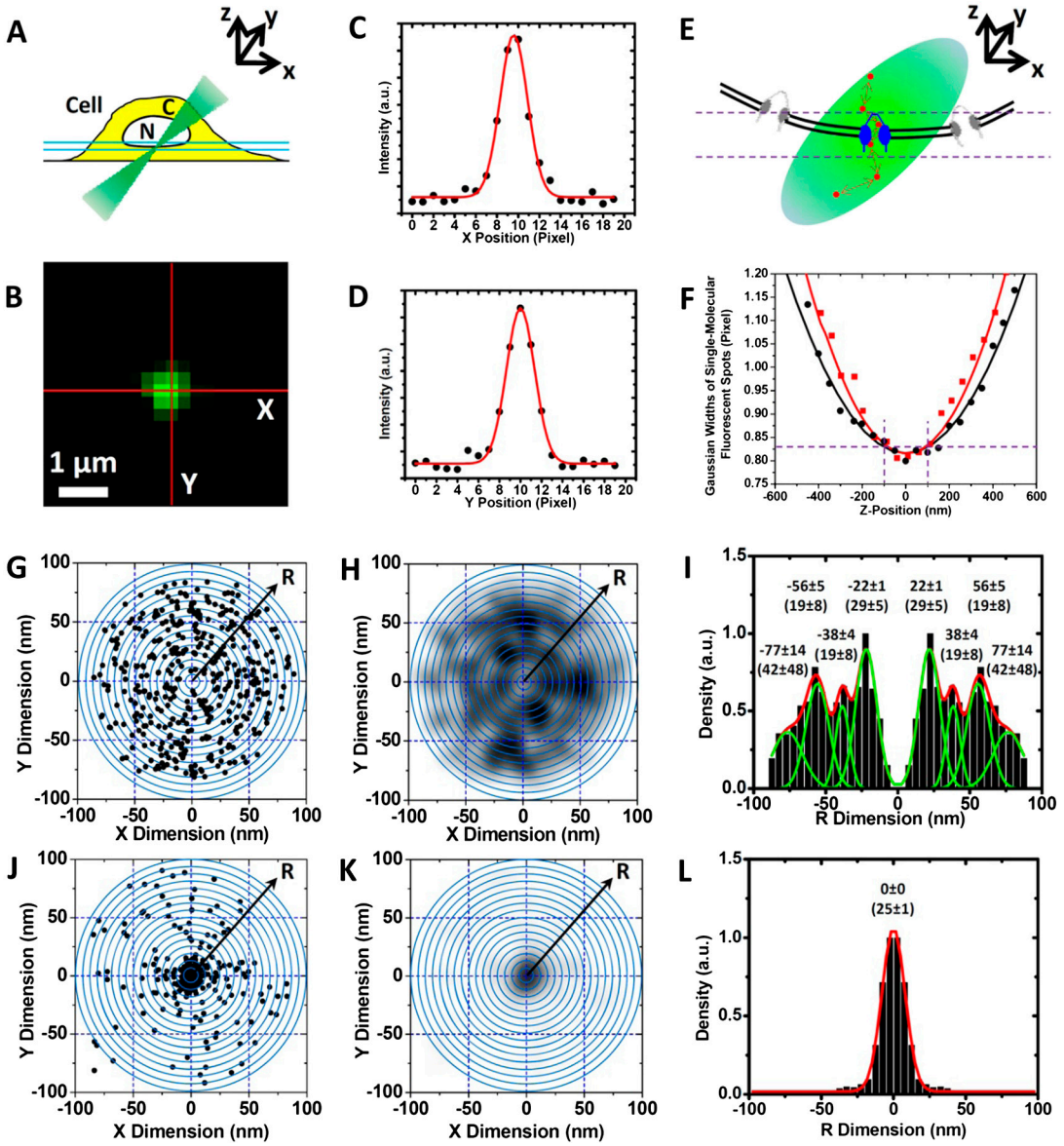

Fig. S2. Illumination of single NPCs at the bottom of NE by SPEED microscopy. (*A*) An off-axis 488-nm excitation laser beam was focused by objective to form an inclined illumination point spread function (iPSF forms an angle of 45° to the z direction) in a cell. C, cytoplasm; N, nucleus. (*B*) Only a single GFP-NPC (green spot) inside the iPSF was excited in all *xyz* dimensions at the bottom plane of HeLa cell nucleus in the focal plane (between the double light blue lines in *A*). Scale bar: 1 μm. (*C* and *D*) The fluorescent spot of the single illuminated GFP-NPC was fit well by a Gaussian function in both *x* and *y* directions. (*E*) Single-molecule imaging and tracking of transiting molecules through the only illuminated GFP-NPC. Followed the same beam path, a second laser was introduced to image and track single transiting molecules (red dots) through the illuminated NPC (blue). C, cytoplasm; N, nucleus. (*F*) Single transiting molecules inside or outside the NPC (moving in *z* direction) were strictly determined based on their Gaussian widths. The relationship between the locations and the Gaussian widths of single transiting molecules in *z* direction indicated that they stayed inside the NPC (−100 to +100 nm as shown by purple lines) if their Gaussian widths are smaller than 0.83 pixel (240 nm per pixel) in SPEED microscopy. Gaussian widths of single molecules changed steeper along the *z* direction in SPEED microscopy (red line and square symbols) than in laser confocal microscopy (LCM, black line and round dots). C, cytoplasm; N, nucleus. (*G*) The obtained 2D spatial locations of Imp β1 molecules in the NPC located at the bottom of NE. To highlight the distribution in radial (R) dimension, 16 concentric rings with 5-nm gaps between neighboring rings was superimposed on the 2D spatial distribution. (*H*) The corresponding 2D probability density map of the spatial locations in G. (*I*) The histogram of densities along the R dimension was fit by multiple Gaussian functions. The peak position and the width (in brackets) at e^{-2} of the Gaussian width were obtained by the fit. (*J*–*L*) The 2D spatial locations, probability density map and histogram for 10-kDa dextran molecules in the NPC.

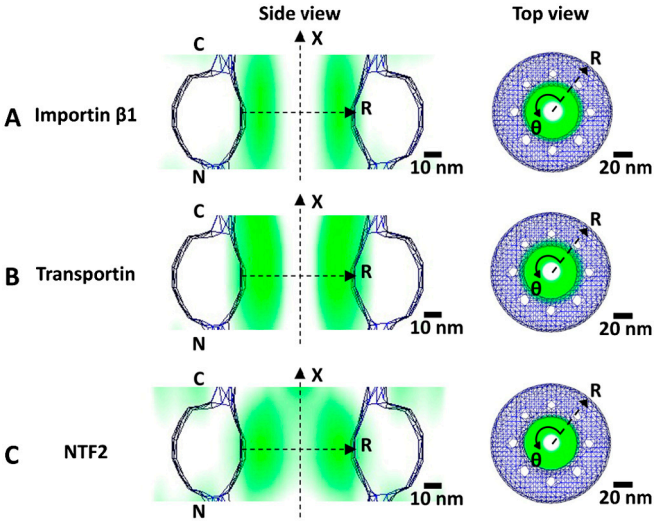

Fig. S3. Three-dimensional pathways for Imp β1, transportin, and NTF2 in native NPCs obtained by SPEED microscopy. Superimposed on the NPC structure, 3D probability density maps (green cloud; brighter color indicates higher density) for Imp β1 (*A*), transportin (*B*), and NTF2 (*C*) in native NPCs were shown in both top view and side view as central slice along the nucleocytoplasmic axis. The cylindrical coordinate system of (x, R, θ) is shown. C, the cytoplasmic side of NPC. N, the nucleoplasmic side of NPC.

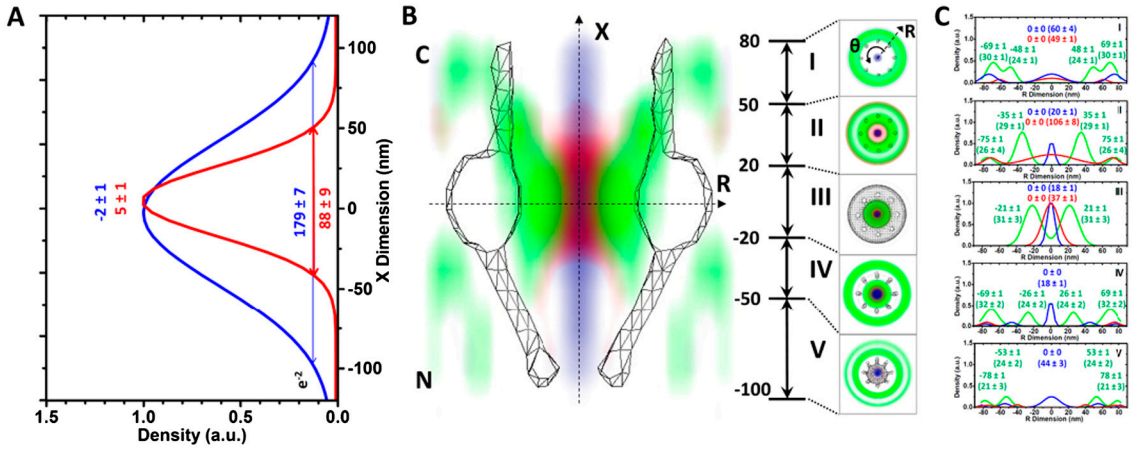

Fig. S4. Superimposed transport routes of passive diffusion and facilitated translocation. (*A*) Length of passive diffusion channel in the NPC. The passive diffusion channels of 0.3 kDa fluorescein (red) and 29 kDa GFP (blue) in the NPC used as examples were determined at the e^{-2} Gaussian width. (*B*) Central slice along the nucleocytoplasmic axis of the 3D probability density maps of 217 kDa labeled import cargo complex of NLS-2xGFP/Imp α/Imp β1 (green cloud), 0.3 kDa fluorescein (red cloud), and 29 kDa labeled GFP (blue cloud), superimposed onto the NPC structure. The cross sections along the R dimension in five distinct regions were marked from I to V with relative distances from the centroid of NPC. All numbers are in nanometers. C, the cytoplasmic side of NPC. N, the nucleoplasmic side of NPC. (*C*) Histograms of probability spatial densities for the above three transiting molecules along the radii (R) at the cross-section of NPC in the range I to V. Major peaks and e^{-2} widths (in brackets) for import cargo complex (green), fluorescein (red) and GFP (blue) were obtained from Gaussian fittings of histograms of probability spatial densities.

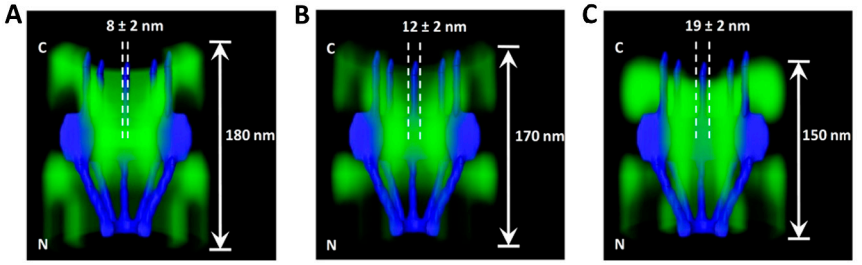

Fig. S5. Three-dimensional pathways of the import cargo complex at 0.5 μM, 3 μM, and 15 μM Imp β1. (*A*) Cut-away view of the 3D spatial density map for the import cargo complex of Imp α/Imp/β1/NLS-2xGFP (green cloud; brighter color indicates higher density) superimposed on the NPC architecture (blue) at 0.5 μM Imp β1. The length of the pathway and the diameter of the rarely occupied tube are labeled in nanometers. (*B*) Cut-away view of the 3D pathways for import cargo complex (green cloud; brighter color indicates higher density) superimposed on the NPC architecture (blue) at 3 μM Imp β1. (*C*) Cut-away view of the 3D spatial density maps for the import cargo complex (green cloud; brighter color indicates higher density) superimposed on the NPC architecture (blue) at 15 μM Imp β1.

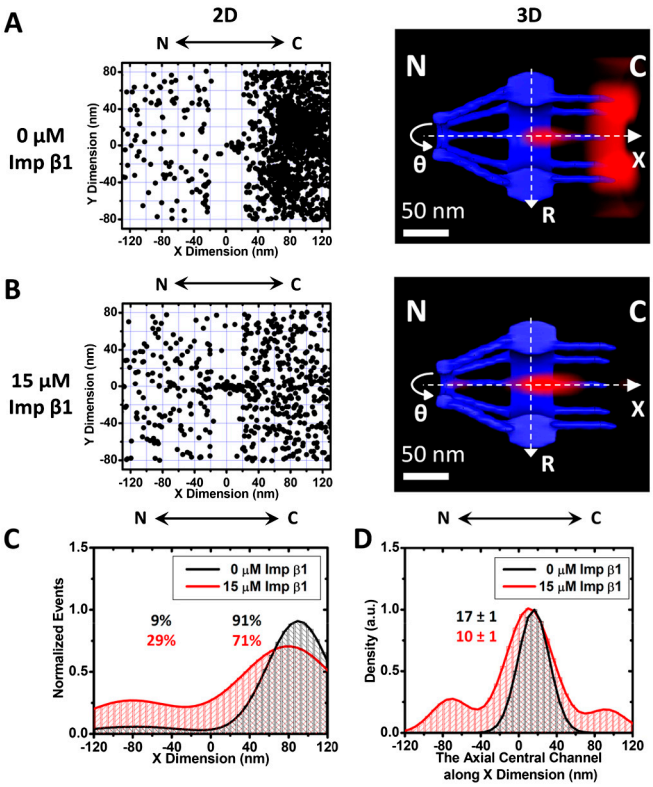

Fig. S6. Nucleocytoplasmic transport route of 70 kDa-dextran molecules at the presence of either 0 μM or 15 μM Imp β1 in permeabilized HeLa cells captured by SPEED microscopy. (*A*) 1-nM labeled 70 kDa-dextran molecules without addition of Imp β1. Superimposed plots of spatial localizations of single dextran molecules located primarily within a rectangular area of 240 x 160 nm around the centroid of NPC. With a 2D to 3D deconvolution process (1), the 3D probability density map (red cloud; brighter color indicates higher density) was obtained and shown in side view superimposed on the NPC architecture (blue). C, the cytoplasmic side of NPC. N, the nucleoplasmic side of NPC. (*B*) Two-dimensional spatial locations and 3D probability density map of 1-nM labeled 70 kDa-dextran molecules with addition of 15 μM Imp β1. (*C*) Percentages of spatial locations of dextran molecules on either side of the NPC at 0 μM (black) or 15 μM Imp β1 (red). The NPC became more permeable for 70-kDa-dextran at 15 μM Imp β1 and 20% more molecules diffused through the central scaffold region. C, the cytoplasmic side of NPC. N, the nucleoplasmic side of NPC. (*D*) The length of central passive diffusion channel at the presence of either 0 μM (black) or 15 μM Imp β1 (red). Based on the Gaussian fits, the length of central channel became longer at the presence of 15 μM Imp β1, and also the peak position of spatial density of dextran molecules along the x dimension shifted from 17±1 nm at 0 μM Imp β1 to 10±1 nm at 15 μM Imp β1 in the NPC. C, the cytoplasmic side of NPC. N, the nucleoplasmic side of NPC.

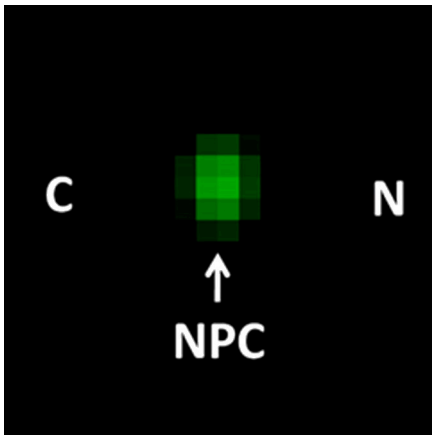

Movie S1. This movie shows a typical import event of Imp β1 from the cytoplasm to the nucleus in a eukaryotic cell. Individual frames of this movie are shown in Fig. S1*A*. Pixels are 240-nm square; each frame was acquired in 400 μs; and the playback speed is 2500X slower than real time. The compartment on the left side of the NPC (the green fluorescent spot) is the cytoplasm (*C*), and the right side is the nucleus (N). The Imp β1 molecule (the red fluorescent spot) starts in the cytoplasm, interacts with the NPC and ends in the nucleus.

Movie S1 (MOV)

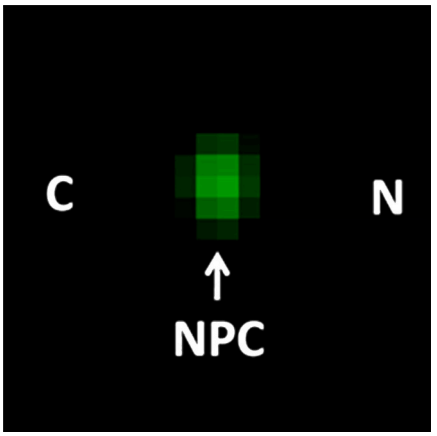

Movie S2. This movie shows a typical export event of Imp β1 from the nucleus to the cytoplasm in a eukaryotic cell. The acquisition time and playing speed are the same as those of Movie S1. The Imp β1 molecule (the red fluorescent spot) starts in the nucleus (N), interacts with the NPC (the green fluorescent spot) and ends in the cytoplasm (C). Individual frames of this movie are shown in Fig. S1*C*.

Movie S2 (MOV)

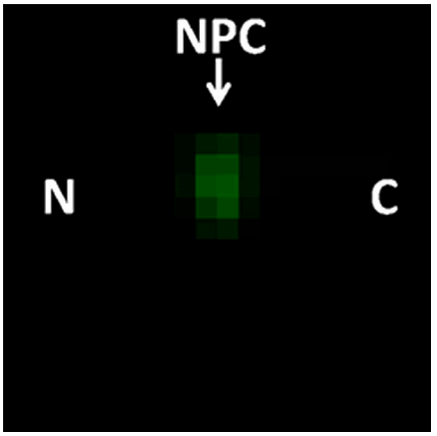

Movie S3. This movie shows a typical import event of cargo complex Imp α/Imp β1/NLS-2xGFP from the cytoplasm to the nucleus in a eukaryotic cell. The acquisition time and playing speed are the same as those of Movie S1. The cargo complex molecule (the red fluorescent spot) starts from the cytoplasm (C), interacts with the NPC (the green fluorescent spot) and ends in the nucleus (N). Individual frames of this movie are shown in Fig. S1*E*.

Movie S3 (MOV)

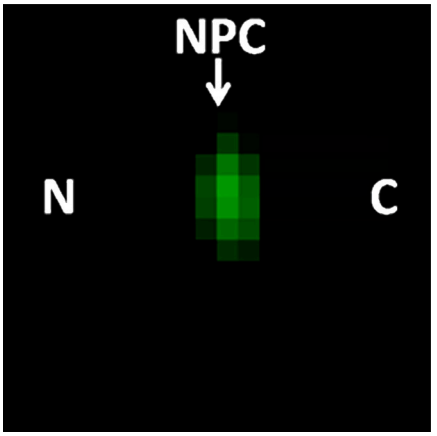

Movie S4. This movie shows a typical import diffusion event of 10 kDa-dextran from the cytoplasm to the nucleus in a eukaryotic cell. The acquisition time and playing speed are the same as those of Movie S1. The dextran molecule (the red fluorescent spot) starts from the cytoplasm (C), diffuses through the NPC (the green fluorescent spot) and ends in the nucleus (N). Individual frames of this movie are shown in Fig. 1*E*.

Movie S4 (MOV)

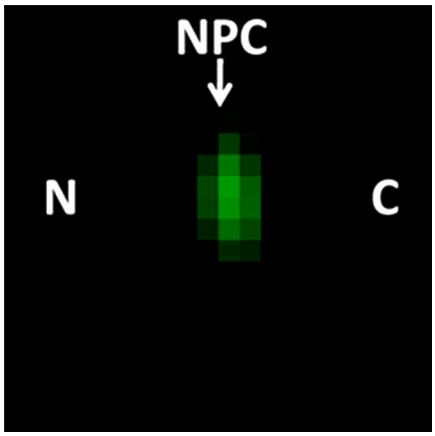

Movie S5. This movie shows a typical export diffusion event of 10 kDa-dextran from the nucleus to the cytoplasm in a eukaryotic cell. The acquisition time and playing speed are the same as those of Movie S1. The dextran molecule (the red fluorescent spot) starts from the nucleus (N), diffuses through the NPC (the green fluorescent spot), and ends in the cytoplasm (C). Individual frames of this movie are shown in Fig. 1*E*.

Movie S5 (MOV)

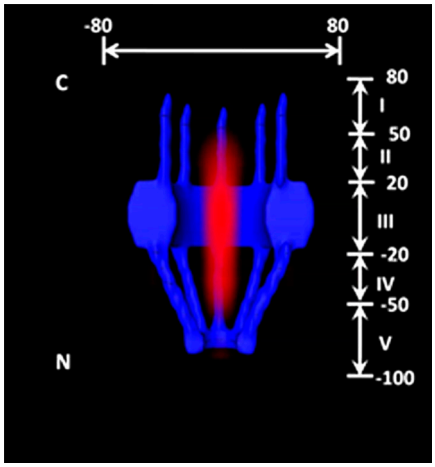

Movie S6. This movie shows a cut-away view of the 3D diffusion pathway for 10 kDa-dextran through the NPC at 1 nM Imp β1 (red cloud; brighter color indicates higher spatial density) superimposed on the NPC architecture (blue). C, the cytoplasmic side of the NPC. N, the nucleoplasmic side of the NPC. Five regions were marked from I to V with the relative distances from the centroid of NPC. Numbers denote distance (nm).

Movie S6 (MOV)

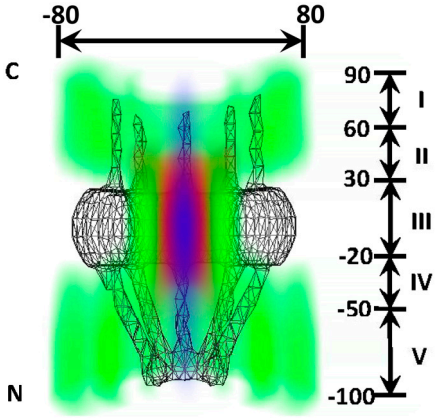

Movie S7. This movie shows a cut-away view of the overlapped 3D pathways of 0.3 kDa-dextran, GFP, and Imp β1 (red, blue, and green clouds for dextran, GFP, and Imp β1, respectively; brighter color indicates higher spatial density) superimposed on the NPC architecture (gray). Based on the spatial locations of effective interaction sites between Imp β1 and the FG-Nups, the NPC can be divided into five regions marked from I to V with the relative distances from the centroid of NPC. Numbers denote distance (nm). C, the cytoplasmic side of NPC. N, the nucleoplasmic side of NPC.

Movie S7 (MOV)

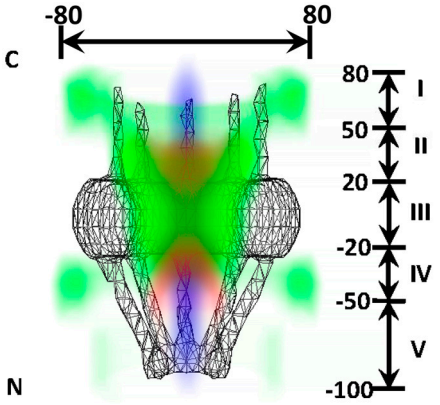

Movie S8. This movie shows a cut-away view of the overlapped 3D pathways of 0.3 kDa-dextran, GFP, and the import cargo complex (Imp α/Imp β1/NLS-2xGFP) (red, blue, and green clouds for dextran, GFP, and Imp β1, respectively; brighter color indicates higher spatial density) superimposed on the NPC architecture (gray). Based on the spatial locations of effective interaction sites between the import cargo complex and the FG-Nups, the NPC can be divided into five regions marked from I to V with the relative distances from the centroid of NPC. Numbers denote distance (nm). C, the cytoplasmic side of NPC. N, the nucleoplasmic side of NPC.

Movie S8 (MOV)

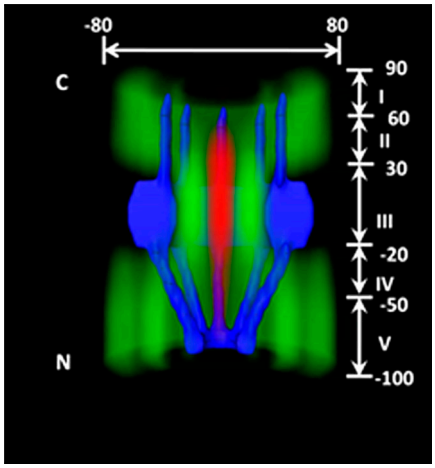

Movie S9. This movie shows a cut-away view of the overlapped 3D pathways of 10 kDa-dextran and Imp β1 at 3 μM Imp β1 (green and red clouds for Imp β1 and dextran, respectively; brighter color indicates higher spatial density) superimposed on the NPC architecture (blue). Based on the spatial locations of effective interaction sites between Imp β1 and the FG-Nups, the NPC can be divided into five regions marked from I to V with the relative distances from the centroid of NPC. Numbers denote distance (nm). C, the cytoplasmic side of NPC. N, the nucleoplasmic side of NPC.

Movie S9 (MOV)

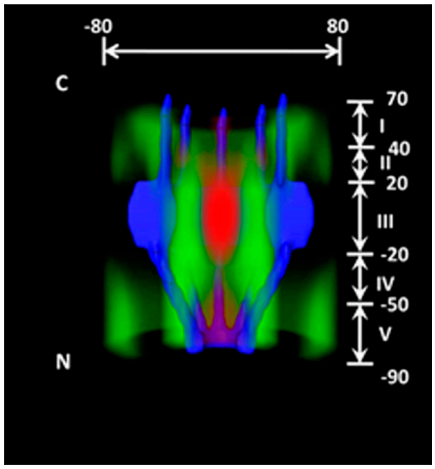

Movie S10. This movie shows a cut-away view of the overlapped 3D pathways of 10 kDa-dextran and Imp β1 at 15 μM Imp β1 (green and red clouds for Imp β1 and dextran, respectively; brighter color indicates higher spatial density) superimposed on the NPC architecture (blue). Based on the spatial locations of effective interaction sites between Imp β1 and the FG-Nups, the NPC can be divided into five regions marked from I to V with the relative distances from the centroid of NPC. Numbers denote distance (nm). C, the cytoplasmic side of NPC. N, the nucleoplasmic side of NPC.

Movie S10 (MOV)

Table S1. Localization precision for immobile and moving substrate molecules obtained at excitation optical density of 500 kW/cm^{-2} and CCD exposure time of 400 μs

	Localization precision (nm)	
Molecule	Immobile	Moving
Fluorescein	12 ± 1	13 ± 1
Alexa Fluor 647	10 ± 1	11 ± 1
Alexa Fluor 488 labeled 3 kDa-dextran	9 ± 1	10 ± 1
Alexa Fluor 647 labeled insulin	10 ± 1	11 ± 1
Alexa Fluor 647 labeled 10 kDa-dextran	10 ± 1	11 ± 1
Alexa Fluor 647 labeled a-lactalbumin	10 ± 1	11 ± 1
Alexa Fluor 647 labeled GFP	12 ± 1	13 ± 1
Fluorescein labeled 40 kDa-dextran	12 ± 1	13 ± 1
Fluorescein labeled 70 kDa-dextran	9 ± 1	10 ± 1
Alexa Fluor 647 labeled NLS-2xGFP	9 ± 1	10 ± 1
Alexa Fluor 647 labeled NTF2	10 ± 1	11 ± 1
Alexa Fluor 647 labeled transportin	10 ± 1	11 ± 1
Alexa Fluor 647 labeled-Imp b1	9 ± 1	10 ± 1

Table S2. Characterization of axial central passive diffusion channel in NPC

		Diameter of molecule (nm)	Diameter of the central channel (nm)			Length of the central channel (nm)			Confinement effect	Calculated time (ms)	Measured time (ms)	Viscosity (cp)
Molecular name	MW (kDa)		e^{-1}	FWHM	e^{-2}	e^{-1}	FWHM	e^{-2}				
Fluorescein	0.3	1.4	19 ± 1	22 ± 1	37 ± 1	44 ± 5	51 ± 5	88 ± 9	1.00 ± 0.02	0.05 ± 0.01	0.2 ± 0.2	3.4 ± 2.1
Alexa Fluor 647	1.3	2.3	13 ± 1	15 ± 1	24 ± 1	63 ± 4	74 ± 5	125 ± 8	1.00 ± 0.02	0.16 ± 0.01	0.5 ± 0.2	3.4 ± 0.7
Alexa Fluor 488 labeled 3 kDa-dextran	4	3.4	11 ± 1	12 ± 2	19 ± 2	70 ± 5	83 ± 6	140 ± 10	0.73 ± 0.06	0.41 ± 0.05	0.8 ± 0.2	2.0 ± 0.4
Alexa Fluor 647 labeld insulin	7	4.0	11 ± 1	12 ± 1	19 ± 1	83 ± 5	98 ± 6	166 ± 10	0.64 ± 0.04	0.74 ± 0.08	1.2 ± 0.2	1.6 ± 0.2
Alexa Fluor 647 labeled 10 kDa-dextran	11	4.6	12 ± 1	13 ± 1	18 ± 1	84 ± 6	99 ± 7	168 ± 12	0.55 ± 0.05	1.08 ± 0.15	1.7 ± 0.2	1.6 ± 0.2
Alexa Fluor 647 labeled a-lactalbumin	15	5.1	11 ± 1	12 ± 1	16 ± 2	84 ± 2	99 ± 2	167 ± 3	0.46 ± 0.04	1.41 ± 0.14	2.2 ± 0.2	1.6 ± 0.2
Alexa Fluor 647 labeled GFP	29	6.3	12 ± 1	13 ± 1	17 ± 1	89 ± 4	106 ± 4	179 ± 7	0.40 ± 0.03	2.34 ± 0.22	4.0 ± 0.2	1.7 ± 0.2
Alexa Fluor 647 labeled 10 kDa-dextran												
at 0 μM Imp β1	11	4.6	9 ± 1	11 ± 1	18 ± 2	84 ± 6	99 ± 7	168 ± 12	0.55 ± 0.05	1.08 ± 0.15	1.7 ± 0.2	1.6 ± 0.2
at 3 μM Imp β1	11	4.6	14 ± 1	16 ± 1	27 ± 2	73 ± 3	86 ± 4	146 ± 6	0.69 ± 0.02	0.64 ± 0.04	0.9 ± 0.2	1.3 ± 0.3
at 15 μM Imp β1	11	4.6	18 ± 1	21 ± 1	35 ± 2	46 ± 4	54 ± 5	92 ± 8	0.78 ± 0.02	0.23 ± 0.03	0.3 ± 0.2	1.3 ± 0.9

The length and diameter of the central channel varied depending on either the size of small molecules or the added Imp β1 concentrations. The detailed description of determination of molecular size and dimension of passive diffusion channel were included in "Determination of Molecular Diameter" and "Gaussian Fittings in the Determination of Dimensions for Transport Routes in the NPC." Confinement effect of a small tube on insert diffusing molecules was derived from ref. 7. For details of transport time and the effective viscosity of the medium in the channel, see the main text.